Available online at www.sciencedirect.com
ScienceDirect
Journal of Power Sources 161 (2006) 1307–1313
JOURNAL OF POWER SOURCES
www.elsevier.com/locate/jpowsour

Characterization of Zn- and Fe-substituted $LiMnO_2$ as cathode materials in Li-ion cells

P. Suresh [a], A.K. Shukla [a], N. Munichandraiah [b,*]

[a] *Solid State and Structural Chemistry Unit, Indian Institute of Science, Bangalore 560012, Karnataka, India*
[b] *Department of Inorganic and Physical Chemistry, Indian Institute of Science, Bangalore 560012, Karnataka, India*

Received 1 April 2006; accepted 8 June 2006
Available online 28 August 2006

Abstract

Layered $LiMn_{1-x}M_xO_2$ (M = Zn or Fe) ($0 \le x \le 0.3$) samples are synthesized from the corresponding sodium analogues by an ion-exchange method using LiBr in *n*-hexanol at 160 °C. The samples are subjected to physicochemical and electrochemical characterization. X-ray diffraction data indicate the formation of layered structures for the $LiMn_{1-x}Zn_xO_2$ samples up to $x = 0.3$ and for $LiMn_{1-x}Fe_xO_2$ samples up to $x = 0.2$. Among these, $LiMn_{0.95}Zn_{0.05}O_2$ and $LiMn_{0.95}Fe_{0.05}O_2$ provide the highest capacity values of 180 and 193 mAh g^{-1}, respectively. Both Zn- and Fe-substituted samples display good capacity retention up to 30 charge–discharge cycles. Electrochemical impedance spectroscopy and galvanostatic intermittent titration data corroborate the results obtained from cyclic volatmmetry and charge–discharge cycling.

Keywords: Substituted $LiMnO_2$; Lithium-ion cells; Cyclic voltammetry; Electrochemical impedance spectroscopy; Capacity

1. Introduction

Among the several positive electrode (cathode) materials for Li-ion batteries, layered $LiCoO_2$ has been investigated extensively as it has stable capacity, good reversibility, and high-rate charge–discharge capability. On the other hand, its high cost and toxicity due to cobalt have prompted investigations into alternative materials [1]. Layered $LiNiO_2$ [2] and $LiMnO_2$ [3–5] have been studied widely as possible candidates. Both $LiNiO_2$ and $LiMnO_2$ are plagued, however, by problems associated with their syntheses and also capacity decay on cycling [6,7]. A detailed examination of various types of manganese oxides for battery electrochemistry has been reported by Thackeray [8]. Layered $LiMnO_2$ synthesized by an ion-exchange method has been found to be promising, but its structural transformation causes a large capacity decay during the initial stages of cycling [9]. In order to ameliorate the performance of $LiMnO_2$, partial substitutions of Mn with Co [10], Ni [11], Al [12], Cr [13], and Mg [14] have been attempted. Substitution of Mn by both Ni and Fe at a low concentration has been reported recently [15].

In the present study, Mn in $LiMnO_2$ is partially substituted by Zn and Fe to obtain $LiMn_{1-x}M_xO_2$ (M = Zn or Fe) ($0 \le x \le 0.3$). The effect of varying concentration of Zn and Fe on the properties of these compounds has not been reported in the literature. In this work, the compounds are prepared by employing the ion-exchange method. Structural and electrochemical characterizations are carried out by means of X-ray diffraction (XRD), scanning electron microscopy (SEM), energy dispersive analysis of X-rays (EDAX), inductively coupled plasma analysis (ICP), surface-area analysis, cyclic voltammetry, charge–discharge cycling, electrochemical impedance spectroscopy (EIS), and galvanostatic intermittent titration (GITT).

2. Experimental

$NaMn_{1-x}M_xO_2$ (M = Zn or Fe) ($0 \le x \le 0.3$) phases were synthesized by preparing a mixed solution comprising stoichiometric amounts of Na_2CO_3 (Sarabhai Chemicals), $Mn(CH_3CO_2)_2{\cdot}4H_2O$ (Spectrochem), $Zn(CH_3COO)_2{\cdot}2H_2O$ (Spectrochem) or $Fe(COO)_2{\cdot}2H_2O$ (synthesized in-house) in double-distilled water. Following rotary evaporation at 80 °C, the solid residue was subjected to grinding for about 30 min, heated in air at 250 °C for 12 h, and finally heated at 700 °C

* Corresponding author. Tel.: +91 80 22933183; fax: +91 80 23600683.
E-mail address: muni@ipc.iisc.ernet.in (N. Munichandraiah).

0378-7753/$ – see front matter © 2006 Elsevier B.V. All rights reserved.
doi:10.1016/j.jpowsour.2006.06.098

for 1 h before quenching to room temperature. The product, $NaMn_{1-x}M_xO_2$ (1 g), was then subjected to ion-exchange by refluxing at 140–160 °C for 8 h in 50 ml of *n*-hexanol that contained of 8 M LiBr to obtain the corresponding $LiMn_{1-x}M_xO_2$.

Chemical analysis of the samples was carried out by ICP employing a Varian Vista-pro CCB spectrometer using accu standards, and by EDAX with a JEOL JSM 5600LV scanning electron microscope. The compounds were characterized by powder X-ray diffraction with Cu Kα as the source on a Siemens D5005 diffractometer. Scanning electron microscopy images were obtained from a JEOL JSM 5600LV instrument and FT-IR spectra were recorded in KBr pellets using a Perkin-Elmer spectrometer model Spectrum 1000.

For electrochemical characterization, electrodes were prepared by mixing the oxide sample, acetylene black and polyvinylidene fluoride (Aldrich) in a weight ratio of 85:10:5. *N*-methyl pyrrolidinone (Aldrich) was used to obtain a paste of this mixture, which was coated on an aluminium foil (0.2 μm thick and 0.75 cm^2 area) that was provided with a tag for electrical connection. The foil was polished previously with emery paper, then cleaned, washed with double-distilled water and dried in a vacuum desiccator. Cells were assembled in an argon atmosphere glove-box (MBraun model UNILAB). Lithium was employed for both counter and reference electrodes. The electrode potentials are reported against the Li/Li^+ reference electrode. The electrolyte was 1 M $LiBF_4$ in a mixture ethylene carbonate and dimethyl carbonate (1:1 by volume). A Celgard (2400) porous polypropylene film was used as the inter-electrode separator.

Cyclic voltamograms were recorded with a EG&G PARC potentiostat/galvanostat (model Versastat). Electrochemical impedance spectra were recorded with a EG&G impedance analyzer model 6310 (excitation signal of 5 mV) in the frequency range 100 kHz to 10 mHz. Galvanostatic charge–discharge cycling was performed using a circuit that consisted of a regulated dc power source, a high resistance and an ammeter in series. Cell voltage was measured using a digital multimeter with high input impedance. Galvanostatic intermittent titration was performed with an Ecochemic potentiostat/galvanostat model Autolab 30.

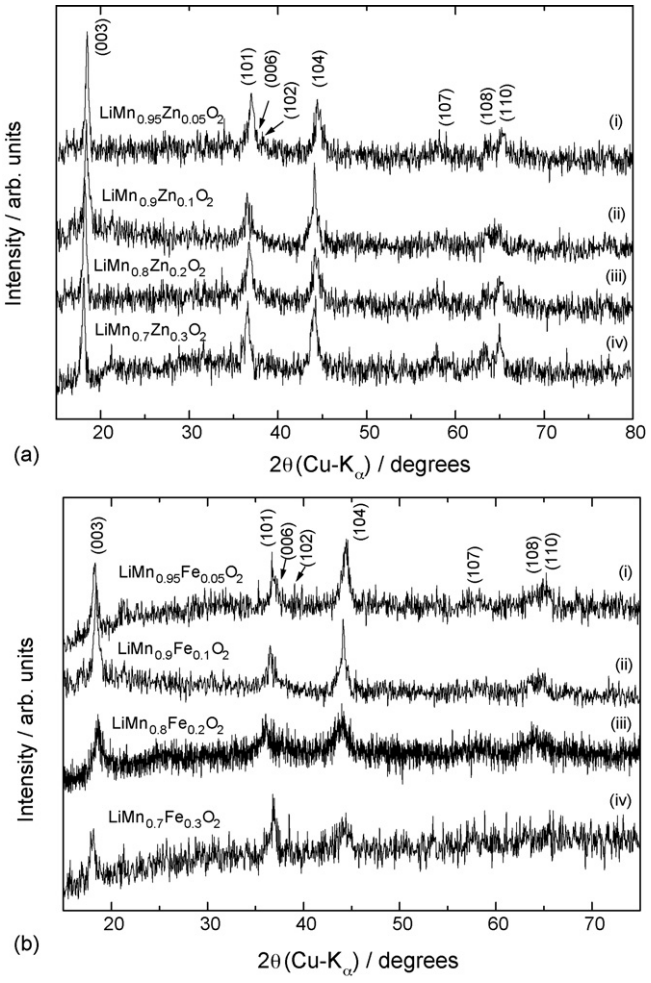

Fig. 1. Powder XRD patterns for (a) Zn-, and (b) Fe-substituted $LiMnO_2$.

3. Results and discussion

Powder XRD patterns of $LiMn_{1-x}M_xO_2$ samples are shown in Fig. 1(a and b), for Zn- and Fe-substituted samples, respectively. The samples exhibited fluorescence. Nevertheless, the patterns obtained for the Zn-substituted samples of *x* from 0.05 up to 0.3 and Fe-substituted samples up to 0.2 could satisfactorily be indexed to a hexagonal unit cell with $R\bar{3}m$ space group.

Although the unit cell of the parent compound, namely $LiMnO_2$ is known to have monoclinic symmetry (*C*2/*m*) [4], the XRD patterns of $LiMn_{1-x}M_xO_2$ obtained in the present work could not be indexed to the *C*2/*m* space group. The best fit of the XRD patterns is obtained only by indexing to a hexagonal unit cell with a $R\bar{3}m$ space group. By contrast, the XRD pattern of $LiMnO_2$ (without substitution) prepared by the present method cannot be indexed to this hexagonal unit cell. These results suggest that $LiMn_{1-x}M_xO_2$ (*x* = Zn and Fe) with compositions of *x* from 0.05 up to 0.3 (Zn substitution) and 0.2 (Fe substitution) is formed with a layered rock-salt structure.

X-ray diffraction patterns of the Zn-substituted samples (Fig. 1(a)) show (1 0 8) (1 1 0) peaks and the peak separation increases with increase in the Zn content, which indicates well-developed layered structures [16]. The lattice parameters (*a* and *c*) were obtained by a least-squares-fitting procedure using the Appleman Program. The values of *a* and *c* are in the range 2.850–2.865 Å and 14.4–14.56 Å, respectively. The *c*/*a* ratio is between 5.035 and 5.075. Furthermore, there is an increase in the values of *a*, *c* and *c*/*a* with an increase in *x*. This increase in *a* and *c* is due to the increased ionic radii of Zn^{2+} in relation to

Table 1
Ionic radii of different metals in various oxidation states assuming an octahedral co-ordination [17]

Ion	Ionic radii (Å) for various oxidation states			
	1+	2+	3+	4+
Li	0.76			
Mn		0.83	0.58	0.53
Zn		0.74		
Fe		0.61	0.55	

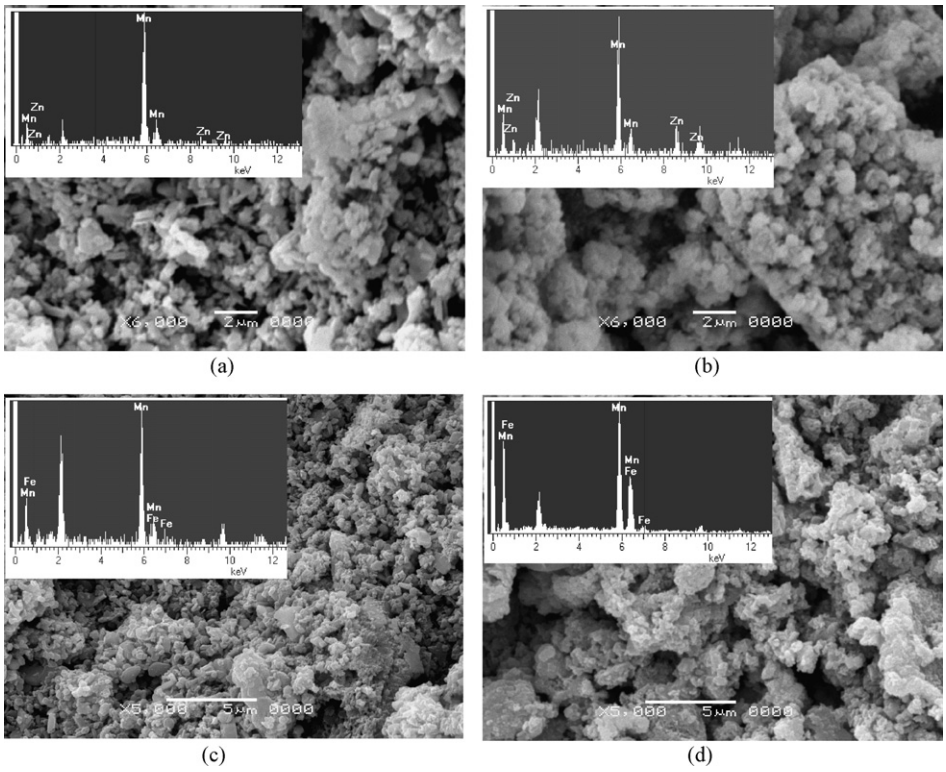

Fig. 2. Scanning electron micrographs for (a) $LiMn_{0.9}Zn_{0.1}O_2$, (b) $LiMn_{0.7}Zn_{0.3}O_2$, (c) $LiMn_{0.9}Fe_{0.1}O_2$, and (d) $LiMn_{0.7}Fe_{0.3}O_2$. Corresponding EDAX patterns are shown in the insets.

Mn^{3+}-ion. The ionic radii values at different oxidation states for Mn, Li, Zn, and Fe are listed in Table 1 [17].

Fe-substituted samples show greater fluorescence than the Zn-substituted counterparts (Fig. 1(b)). Unlike in the case of Zn substitution, it is seen that as the Fe content increases the separation between (1 0 8) and (1 1 0) decreases; the peaks almost merge at $x = 0.3$, and this indicates a gradual transformation of the layered structure to a spinel phase. Lattice parameters were obtained for the Fe-substituted samples up to $x = 0.2$ by indexing the XRD data to a hexagonal unit cell. Parameters a and c, as also c/a ratio are virtually invariant with Fe content. This is because the ionic radius of Fe^{3+} is nearly the same as that of Mn^{3+} (Table 1). The XRD data of all samples, as discussed above, suggest that the layered structures are obtained for Zn substitution up to $x = 0.3$, and for Fe substitution up to $x = 0.2$. The synthesis and characterization of the compounds in the present study are restricted to these compositions because there is a decrease in charge–discharge capacity with increase in concentration of Zn or Fe, as discussed below.

The compositional analyses of the above phases were carried out using ICP and EDAX. Typical, scanning electron micrographs of the samples $LiMn_{0.9}M_{0.1}O_2$ and $LiMn_{0.7}M_{0.3}O_2$ for the Zn and Fe substituents are shown in Fig. 2. The EDAX pattern for each sample is also shown. The images reveal agglomeration of sub-micron size particles, which results in poor crystallinity as reflected in the XRD-patterns (Fig. 1). By contrast, the XRD patterns of the sodium phases (not shown) contained intense peaks and the SEM images showed particles of good crystallinity. Hence, as expected, there is a decrease in crystallinity of the sample during ion-exchange [15]. The compositions estimated form the analyses are compared with the target compositions in Table 2. It is noted that the total alkali metal concentration is about 10% lower than the expected composition, as reported by others [11]. Furthermore, the concentration of Na is negligibly small, which indicates that Na^+/Li^+ ion-exchange is close to completion.

The FTIR spectra of the $LiMn_{1-x}M_xO_2$ (M = Zn, Fe) samples for $x = 0.1$ and 0.3 (Fig. 3). It is seen that the spectra of the samples are similar and that there are three bands at 440, 510, 630 cm^{-1} in the region 400–800 cm^{-1}, except in the case of $LiMn_{0.7}Fe_{0.3}O_2$. The last-mentioned sample shows splitting of the 510 cm^{-1} band into two bands at 483 and 522 cm^{-1}. These bands are assigned to M–O bonds. As predicted by group theory [18], four bands should be observed in the region 200–900 cm^{-1} for layered compounds with a $R\bar{3}m$ space group, and five bands for the spinel. For the layered compound, a band

Table 2
Intended and observed compositions of substituted $LiMnO_2$

Intended composition	Observed composition
$LiMn_{0.95}Zn_{0.05}O_2$	$Na_{0.012}Li_{0.889}Mn_{0.937}Zn_{0.063}O_2$
$LiMn_{0.9}Zn_{0.1}O_2$	$Na_{0.013}Li_{0.886}Mn_{0.889}Zn_{0.111}O_2$
$LiMn_{0.8}Zn_{0.2}O_2$	$Na_{0.009}Li_{0.883}Mn_{0.787}Zn_{0.213}O_2$
$LiMn_{0.7}Zn_{0.3}O_2$	$Na_{0.013}Li_{0.873}Mn_{0.712}Zn_{0.288}O_2$
$LiMn_{0.95}Fe_{0.05}O_2$	$Na_{0.01}Li_{0.897}Mn_{0.941}Fe_{0.059}O_2$
$LiMn_{0.9}Fe_{0.1}O_2$	$Na_{0.009}Li_{0.876}Mn_{0.897}Fe_{0.103}O_2$
$LiMn_{0.8}Fe_{0.2}O_2$	$Na_{0.015}Li_{0.865}Mn_{0.776}Fe_{0.224}O_2$
$LiMn_{0.7}Fe_{0.3}O_2$	$Na_{0.013}Li_{0.867}Mn_{0.718}Fe_{0.282}O_2$

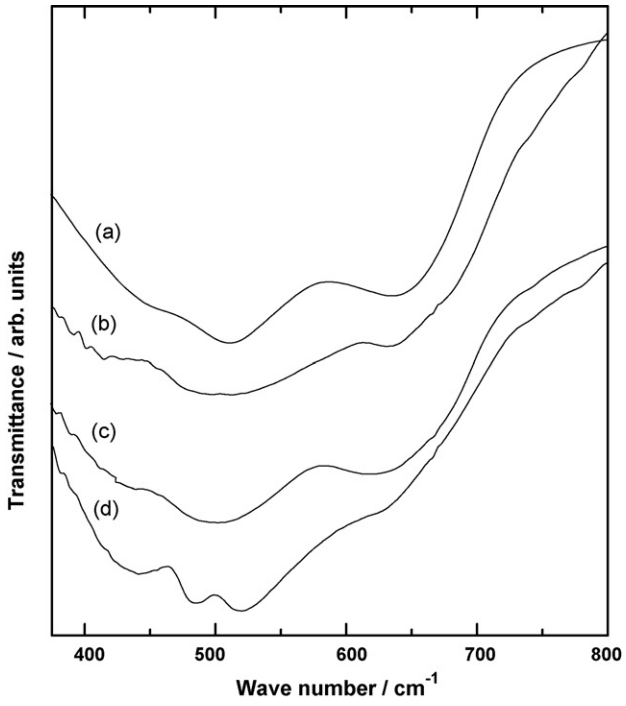

Fig. 3. FTIR spectra for (a) $LiMn_{0.9}Zn_{0.1}O_2$, (b) $LiMn_{0.7}Zn_{0.3}O_2$, (c) $LiMn_{0.9}Fe_{0.1}O_2$, and (d) $LiMn_{0.7}Fe_{0.3}O_2$.

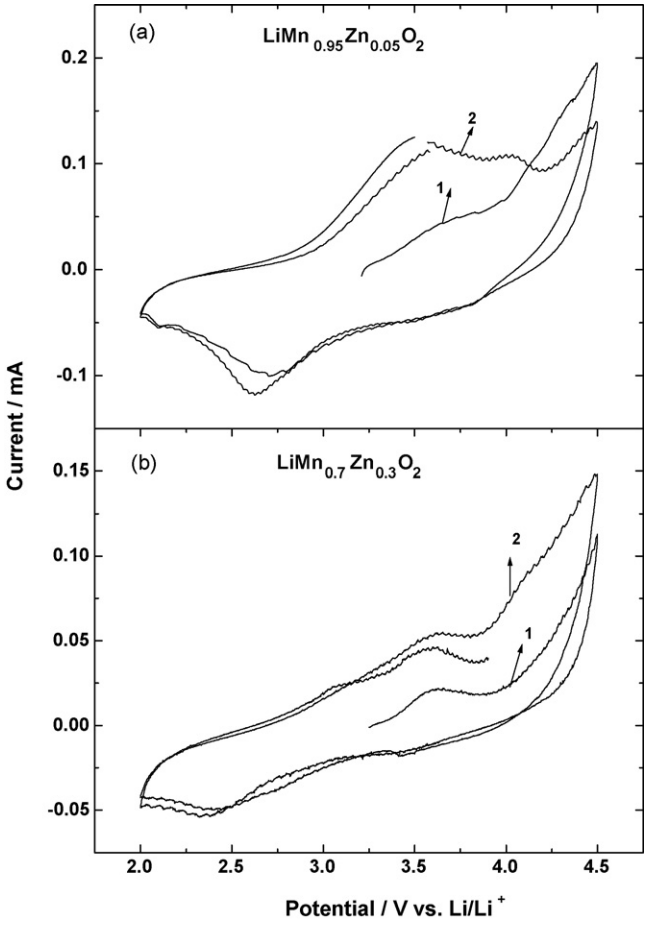

Fig. 4. Cyclic voltammograms for (a) $LiMn_{0.95}Zn_{0.05}O_2$, and (b) $LiMn_{0.7}Zn_{0.3}O_2$. Scan rate = 50 μV s^{-1}. Material weight = 5 mg.

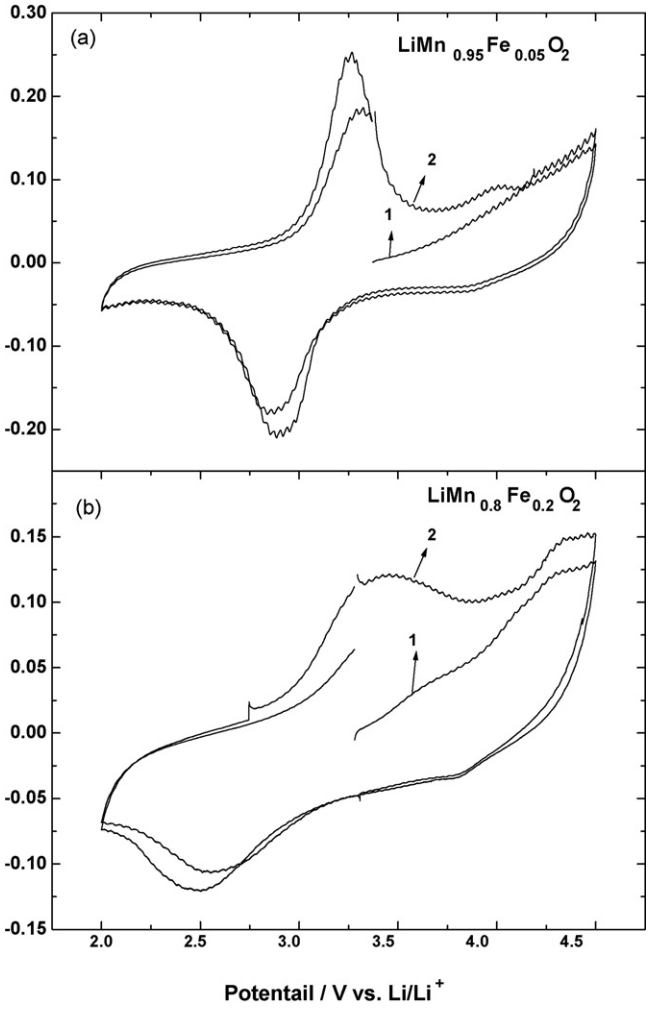

Fig. 5. Cyclic voltammograms for (a) $LiMn_{0.95}Fe_{0.05}O_2$, and (b) $LiMn_{0.8}Fe_{0.2}O_2$. Scan rate = 50 μV s^{-1}. Material weight = 5 mg.

is expected at 270 cm^{-1} in addition to the three bands but that region is not investigated in the present experiment due to limitation of the spectrometer. Hence, Zn-substituted samples have layered structures for compositions up to $x = 0.3$. In the case of Fe-substituted samples, however, transformation to a spinel structure is observed with increase in Fe content to $x = 0.3$ [19].

Cyclic voltammograms were recorded for the electrodes in the voltage range 2–4.5 V at a scan rate of 50 μV s^{-1}. Voltammograms for the Zn- and Fe-substituted samples are shown in Figs. 4 and 5, respectively. $LiMn_{0.95}Zn_{0.05}O_2$ (Fig. 4(a)) has an anodic peak at 3.5 V with a corresponding cathodic peak at 2.6 V; these peaks are assigned to a Mn^{3+}/Mn^{4+} redox couple. For $LiMn_{0.7}Zn_{0.3}O_2$, a decrease in peak current is observed for both anodic and cathodic peaks (Fig. 4(b)). The decrease in peak intensity is due to a decrease in the electrochemically active Mn^{3+}-ions with an increase in Zn^{2+}-ions in the sample.

Cyclic voltammograms for the Fe-substituted samples are shown in Fig. 5. For $LiMn_{0.95}Fe_{0.05}O_2$, an anodic peak appears at 3.25 V (Fig. 5(a)) and a corresponding cathodic peak at 2.9 V. This compound provides sharp current peaks with the highest peak intensities compared with the others compounds. As

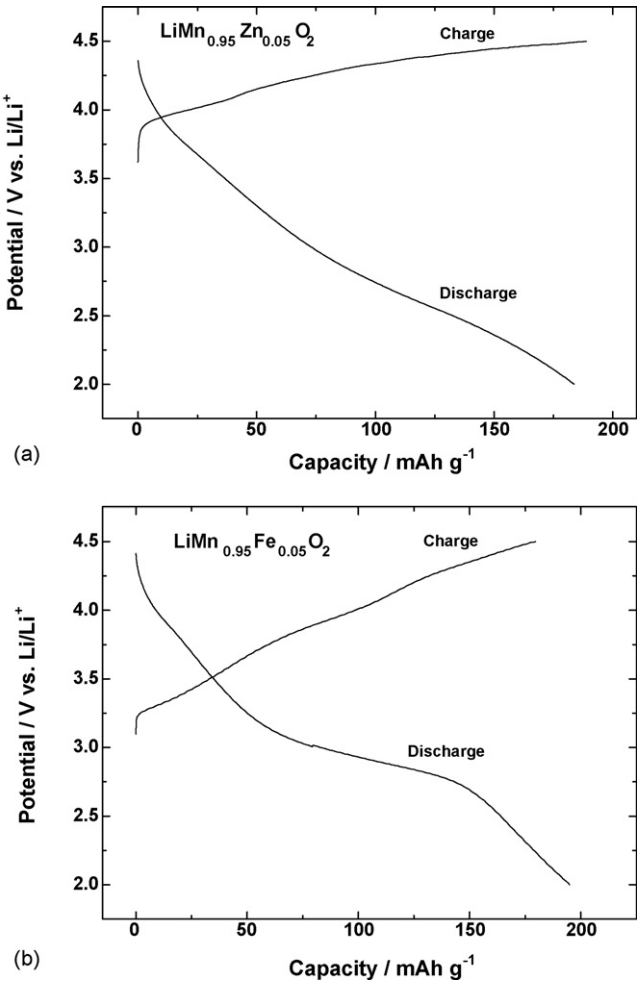

Fig. 6. Charge and discharge profiles for cells with (a) $LiMn_{0.95}Zn_{0.05}O_2$, and (b) $LiMn_{0.95}Fe_{0.05}O_2$ cathodes.

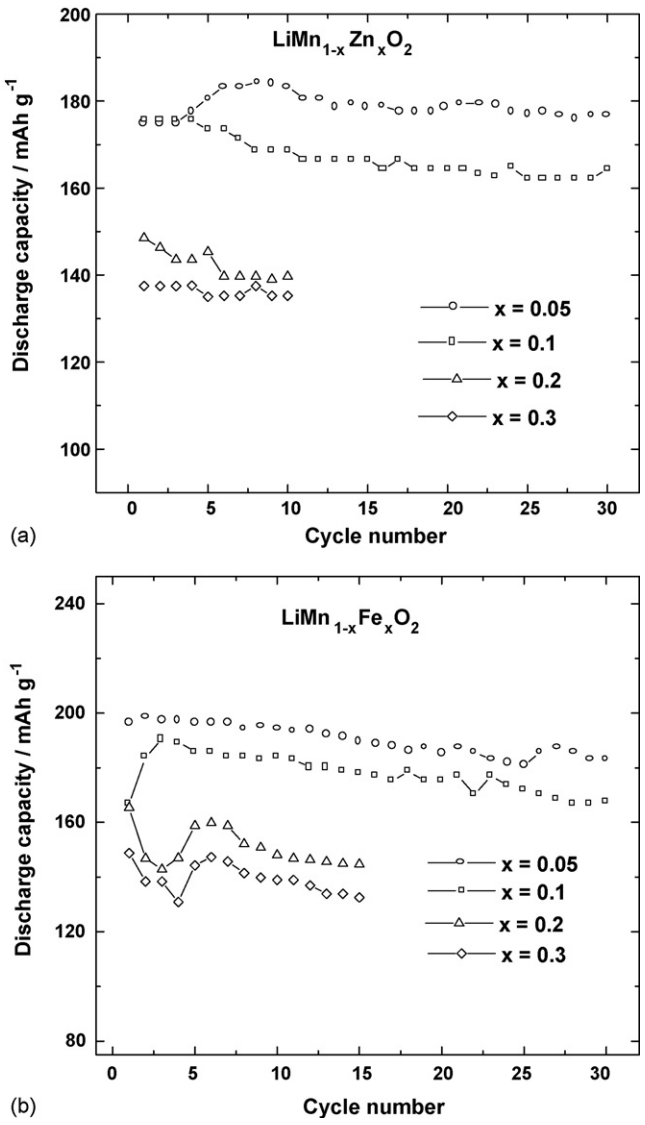

Fig. 7. Cycle-life data for (a) Zn-, and (b) Fe-substituted $LiMnO_2$.

discussed below, the discharge capacity of $LiMn_{0.95}Fe_{0.05}O_2$ is the highest obtained in the present study. For the sample with $x = 0.2$, there is an anodic peak at 3.5 V and a slight hump at 4.5 V with the main cathodic peak at 2.5 V (Fig. 5(b)). The peaks at low potentials are assigned to the Mn^{3+}/Mn^{4+} couple. The peak at 4.5 V is dominant for the compound $LiMn_{0.7}Fe_{0.3}O_2$ (not shown), and correspond to the Fe^{3+}/Fe^{4+} couple in the spinel [20]. With increase in Fe content, the intensity of the anodic peak at 4.5 V increases.

Galvanostatic charge–discharge cycling of all samples was carried out in the potential region between 2 and 4.5 V. Typical voltage profiles during cycling of the oxides $LiMn_{0.95}Zn_{0.05}O_2$ and $LiMn_{0.95}Fe_{0.05}O_2$ are shown in Fig. 6. While charging the Zn-substituted oxide cathodes (Fig. 6(a)), there is a gradual increase of potential from 3.8 to 4.5 V. During discharge, there is a gradual decrease in potential from 4.3 to 2 V (Fig. 6(a)). During charging of $LiMn_{0.95}Fe_{0.05}O_2$ (Fig. 6(b)), there is an increase of potential from 3.25 to 4.5 V. During discharge, there is a plateau at about 3 V.

Cycle-life tests were performed for all samples and the data for the Zn- and Fe-substituted samples are given in Fig. 7(a and b), respectively. The Zn-substituted samples show initial capacities of 185, 170, 150, and 138 mAh g^{-1} for $x = 0.05$, 0.1, 0.2, and 0.3 samples, respectively (Fig. 7(a)). The samples show good capacity retention up to 30 charge–discharge cycles in the case of $x = 0.05$ and 0.1. Fe-substituted samples have initial capacities of 200, 180, 150, and 140 mAh g^{-1} for $x = 0.05$, 0.1, 0.2, and 0.3 samples, respectively. Fe-substituted samples also exhibit good capacity retention up to 30 cycles (Fig. 7(b)). The decrease in capacity with increase in Zn content is due to the decrease in electrochemically active Mn^{3+}-ions, whereas the decrease in capacity with increase of Fe content is attributed to an increase in the amount of Fe that occupies Li sites that thereby gives raise to a modified spinel at higher Fe substitutions.

Electrochemical impedance spectroscopy has been used extensively for evaluation of batteries and electrode materials for battery application. Subsequent to stabilization of the capacity of the electrodes in the present study, impedance spectra were recorded at the charged (i.e., state-of-charge, SOC = 1) and at discharged (SOC = 0) condition. Typical plots for the two electrodes are presented in Fig. 8. Each spectrum consists of a

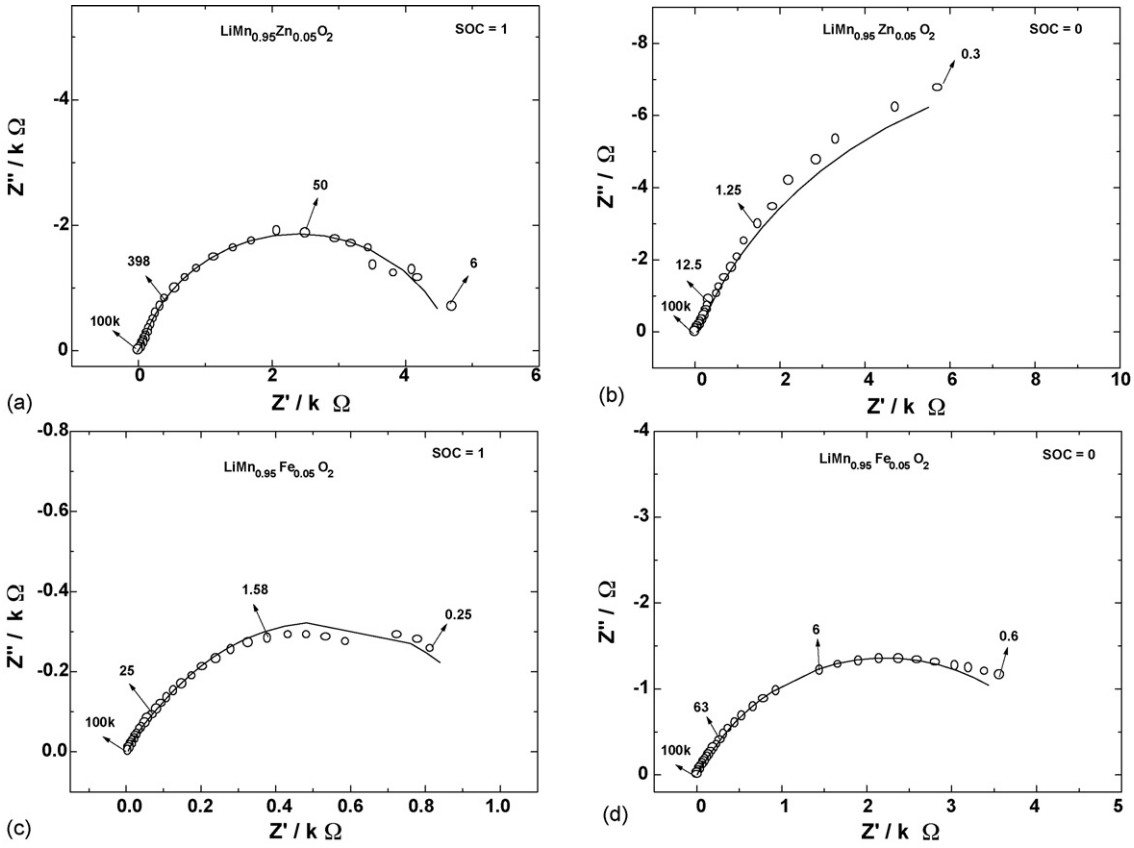

Fig. 8. Nyquist plots of impedance spectra for $LiMn_{0.95}Zn_{0.05}O_2$ at (a) SOC ≈ 1 and (b) SOC ≈ 0, and for $LiMn_{0.95}Fe_{0.05}O_2$ at (c) SOC ≈ 1 and (d) SOC ≈ 0. Experimental data are shown as symbols and theoretical data obtained from NLLS fit results as solid curves. Some of the frequency values are given in Hertz.

high-frequency intercept on the real axis, and a broad semicircle. The high-frequency intercept indicates the ohmic resistance (R_s). Two semicircles have been reported for positive electrodes of Li-ion cells [21]. The broad, distorted semicircle is likely due to overlap of two semicircles. The high-frequency semicircle is associated with the surface film resistance and the diameter of the low-frequency semicircle represents the charge-transfer resistance (R_{ct}) of the electrochemical process.

The impedance spectra of all the compounds at all SOC values were fitted to an equivalent circuit with a circuit code of $R(RQ)(RQ)$, where Q is a constant phase element, similar to the procedure described earlier [22]. The charge-transfer resistance at the fully-charged state (SOC = 1) is plotted against the composition along with the average discharge capacity in the Fig. 9 for the Fe-substituted samples. It is seen that as the concentration of Fe increases, the charge-transfer resistance increases and the average discharge capacity decreases.

In the galvanostatic intermittent titration technique, a $LiMn_{1-x}M_xO_2$ electrode of known composition, say y, with respect to Li, that is, y in Li_y, was subjected to lithiation and de-lithiation by applying a constant current (I_o) for a time τ, at the end of which the compound attained a known lithium content $y \pm \Delta y$. As a result, there was a change in the equilibrium potential (E_o), which reaches E_τ at a time τ. After interruption of the current at time τ, the electrode was allowed to attained its new steady-state potential E_s, and the change in this potential ΔE_s ($=E_s - E_o$) was calculated. From the values of ΔE_τ ($=E_\tau - E_o$) and ΔE_s, the diffusion co-efficient of Li (D_{Li}) was calculated using Eq. (1) [23], for several SOC values.

$$D_{Li} = \left(\frac{4}{\pi\tau}\right)\left(\frac{m_B V_m}{M_B A}\right)^2\left(\frac{\Delta E_s}{\Delta E_\tau}\right)^2 \quad (1)$$

In Eq. (1), m is the mass of the active material, M_B the molar mass, V_m the molar volume, and A is geometric area of the electrode. As the true area of the electrode is expected to be greater than the geometric area, D_{Li} is considered to

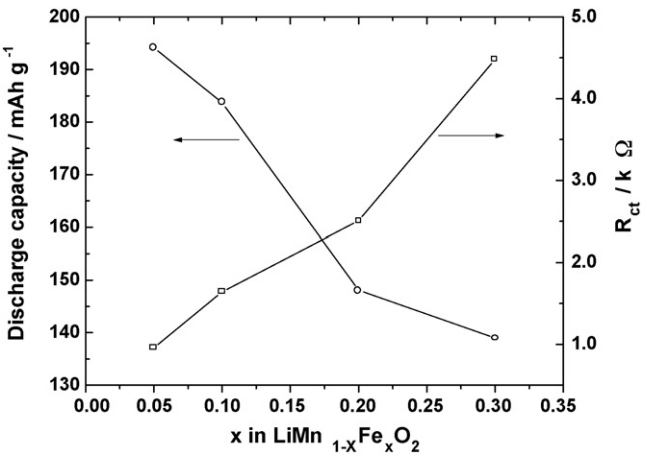

Fig. 9. Variation in charge-transfer resistance (R_{ct}) at SOC ≈ 1 of electrodes and average discharge capacity with composition (x) of $LiMn_{1-x}Fe_xO_2$.

be the 'apparent' diffusion coefficient of Li. Typical experimental values are: $I_o = 25\ \mu A\ cm^{-2}$; $\tau = 5400\ s$; $\Delta E_s = 124\ mV$; $\Delta E_\tau = 252\ mV$; $V_m = 20.8\ cm^3$; $m_B = 2\ mg\ cm^{-2}$. The diffusion coefficient values were obtained for the Zn- and Fe-substituted compounds for $x = 0.1$, at different potentials. The apparent diffusion co-efficient ranges between 10^{-11} and $10^{-13}\ cm^2\ s^{-1}$, and the values agree well with those reported for layered compounds [24].

4. Conclusions

Layered $LiMn_{1-x}M_xO_2$ (M = Zn or Fe) ($0 \le x \le 0.3$) samples have been synthesized from the corresponding sodium analogues by an ion-exchange method using LiBr in *n*-hexanol at 160 °C. The samples have been characterized both physicochemically and electrochemically. Although XRD patterns exhibit a large fluorescence, the data indicate the formation of layered structures for the Zn-substituted samples up to $x = 0.3$ and for Fe-substituted samples up to $x = 0.2$. The $LiMn_{0.95}Zn_{0.05}O_2$ and $LiMn_{0.95}Fe_{0.05}O_2$ samples yield the highest capacity values, namely 180 and 193 mAh g^{-1}, respectively. Both the Zn- and Fe-substituted samples exhibit good capacity retention up to 30 cycles. Zn-substitution improves the capacity retention, but increase in the amount of Zn is detrimental to the achievable capacity. Fe-substitution is found to be beneficial in terms of both capacity retention and achievable capacity, at low concentrations. An increase in the amount of Fe leads to a structural transformation towards the spinel phase because of the tendency of Fe^{3+}-ions to occupy lithium layers.

References

[1] B. Ammundsen, J.M. Paulsen, Adv. Mater. 13 (2001) 943.
[2] T. Ohzuku, A. Ueda, M. Nagayama, Y. Iwakashi, H. Komori, Electrochem. Acta 38 (1993) 1159.
[3] L. Corguennec, P. Denimard, R. Brec, J. Electrochem. Soc. 144 (1997) 332.
[4] A.R. Armstrong, P.G. Bruce, Nature 381 (1996) 499.
[5] H. Wang, Y.I. Jang, B. Huang, D.R. Sadoway, Y.M. Chiang, J. Electrochem. Soc. 146 (1999) 473.
[6] P.G. Bruce, A.R. Armstrong, R. Gitzendanner, J. Mat. Chem. 9 (1999) 193.
[7] J.R. Dahn, E.W. Fuller, M. Obravac, U. von Sacken, Solid State Ionics 69 (1994) 265.
[8] M.M. Thackeray, Prog. Solid State Chem. 25 (1997) 1.
[9] G. Vitins, K. West, J. Electrochem. Soc. 144 (1997) 2587.
[10] A.D. Robertson, A.R. Armstrong, A.J. Fowkes, P.G. Bruce, J. Mat. Chem. 11 (2001) 113.
[11] T.E. Quine, M.J. Duncan, A.R. Armstrong, A.R. Robertson, P.G. Bruce, J. Mater. Chem. 10 (2000) 2838.
[12] Y.I. Jang, B. Huang, Y.M. Chiang, D.R. Sadoway, Electrochem. Solid State Lett. 1 (1998) 13.
[13] I.J. Davidson, R.S. McMillan, J.J. Murray, J. Power Sources 54 (1995) 205.
[14] P. Suresh, A.K. Shukla, N. Munichandraiah, J. Electrochem. Soc. 152 (2005) A2273.
[15] P. Suresh, A.K. Shukla, N. Munichandraiah, Electrochem. Solid State Lett. 8 (2005) A263.
[16] S.C. Garcia, A.C. Couceiro, M.A.S. Rodriguez, F. Soulette, C. Julien, Solid State Ionics 156 (2003) 15.
[17] D.R. Lide (Ed.), CRC Handbook of Chemistry and Physics, 82nd ed., CRC Press, Boca Raton, FL, 2001.
[18] W. Huang, R. Frech, Solid State Ionics 86 (1996) 395.
[19] P. Suresh, A.K. Shukla, N. Munichandraiah, Solid State Ionics 176 (2005) 281.
[20] M.Y. Song, D.S. Ahn, S.G. Kang, S.H. Chang, Solid State Ionics 111 (1998) 237.
[21] M.G.S.R. Thomas, P.G. Bruce, J.B. Goodenough, J. Electrochem. Soc. 132 (1985) 1521.
[22] P. Suresh, A.K. Shukla, N. Munichandraiah, J. Appl. Electrochem. 32 (2002) 267.
[23] K.M. Shaju, G.V. Subbarao, B.V.R. Chowdari, J. Electrochem. Soc. 150 (2003) A1.
[24] Y.M. Choi, S. Pyun, J.S. Bae, S.I. Moon, J. Power Sources 56 (1995) 25.